A unified approach to cirrus microphysics, remote sensing and climate prediction, and its impact in a climate model.

Anthony J. Baran[a], Peter Hill[a], Jerome Vidot[b], Kalli Furtado[a], Paul Field[a], and James Manners[a]

[a]*Met Office, FitzRoy Road, Exeter, Devon, EX1 3PB, U. K.*
[b]*Centre de Météorologie Spatiale, DP/Météo-France, Lannion, France*

Abstract. It is usually the case that current operational climate models are inconsistent between the cirrus microphysics and radiation schemes. This inconsistency arises because the two schemes generally assume different particle size distributions (PSD) and mass-dimensional relationships. Moreover, the couple between the two schemes is generally achieved through some dependence on a diagnosed quantity, such as the "effective dimension," D_e. The calculated values of D_e in the two schemes are also likely to be different (due to different ice crystal shapes and PSDs being assumed). It is physically preferable to unify assumptions between the cirrus microphysics and radiation schemes in the climate model. In this short communication, it is shown that there is no need to use a diagnosed quantity to couple the cirrus microphysics to the radiation scheme, rather this is achieved through a model prognostic variable, the ice mass mixing ratio, whilst maintaining consistency between the two schemes by assuming the same PSDs and mass-dimensional relationship. Moreover, to optimize the radiation scheme in the climate model use is made of global space-based observations in the terrestrial window region to constrain the idealized ensemble. The optimized ensemble is then parametrized and applied to the Met Office Unified Global Atmosphere 6 configuration (GA6). It is shown, relative to the next operational version of the Met Office GA model, that such a unified approach leads to an improvement in the 20 year-averaged Summer (June-July-August) short-wave and long-wave flux at TOA and the temperature structure of the tropical troposphere, when compared against current observations.

Keywords: Climate, Cloud physics, Ice crystals, General circulation model, Radiative schemes, Remote sensing.

INTRODUCTION

The current cirrus bulk ice optical parameterization [1] applied in the Met Office operational Unified Global Atmosphere model is based on the ice aggregate model of [2]. The bulk scalar ice optical properties (i.e., mass extinction coefficient K_{ext}, single-scattering albedo ω_0, and the asymmetry parameter g) in Ref. [1] were calculated using historical in-situ measured PSDs, which were likely skewed to higher concentrations of small ice due to the shattering of ice crystals on or at the inlets of microphysical probes [3, 4]. In [1] K_{ext} is parameterized as a function of ice mass mixing ratio (q_{cf}) and D_e. Since the cloud scheme in the Met office Unified Model is a single-moment scheme, only q_{cf} is predicted, and D_e must be diagnosed through some deterministic polynomial fit to cloud temperature. The problem with this parameterization approach is that the PSDs differ between the prognostic cloud and radiation schemes, and the mass-dimensional relationship also differs between the two schemes. Moreover, the predicted D_e values calculated for the same q_{cf} and temperature values are different in the Met Office models, and the PSDs on which the parameterization of D_e is based were skewed due to ice crystal shattering. This inconsistency is not acceptable in global atmospheric models that are used to predict future atmospheric states, the results of which are used to inform policy makers [5]. It is more desirable to achieve consistency between the global model ice cloud prognostic variable and bulk ice scalar optical properties through assuming the same PSDs and mass-dimensional relationships, without the need to assume a diagnosed coupling between the two schemes. Moreover, a further improvement to the global model parameterization can be achieved if these same assumptions are also demonstrated to agree with global space-based radiometric observations. If the cirrus microphysics, radiation and remote sensing can be unified in such a way, then we can be confident that a representative parameterization is being applied in the global model that should improve prediction of outgoing fluxes at TOA. This overarching philosophy of approach is tested in this short communication.

The Couple between Cirrus Microphysics and the Bulk Scalar Optics

The basis of the parameterization is the ensemble model of cirrus ice crystals proposed by [6]. The model consists of a habit mixture of six different idealized ice crystal shapes. The idealized shapes consist of the hexagonal ice column of aspect ratio unity, followed by the six-branched bullet rosette. Thereafter, hexagonal monomers are randomly attached to build up longitudinal chains of hexagonal ice aggregates consisting of three, five, eight and finally ten-branched aggregates. For each size bin in the PSD, the habit mixture can be assigned weights to each of the models, so that the reflection and transmission properties of the cloud can be biased towards the hexagonal ice columns for the smaller particles or the elongated ice aggregates for the larger particles. The determination of these weights through the use of remote sensing is discussed in the next section. Of course, for each size bin, the sum of weights must add to unity. Other habit mixture models have been proposed such as Refs. [7, 8], but these are not considered here as they are not part of the standard parameterizations used in the forward modeling described in the next section.

To parameterize the bulk scalar optical properties a PSD is required to obtain the volumetric optical properties. The PSD used here is the moment estimation parameterization developed by [9]. In this parameterization, the second moment (i.e., ice mass(D)=aD^b, where D is the maximum dimension of the ice crystal) is related to all other moments via a polynomial fit, which includes the in-cloud temperature. The parameterization developed by [9] is based on 10000 in-situ measurements of the PSD at temperatures between about 0^oC and -60^oC obtained from a number of field campaigns. To reduce the effect of shattering on the parameterization Ref. [9] applied the technique of filtering by applying the method described in Ref. [3], and ice crystals less than 100 μm were ignored but the parameterizations assumes an exponential PSD for sizes less than 100 μm, which is added to a gamma function to complete the PSD. The current Met Office operational global model assumes the PSD parameterization developed by [10], which is based on PSDs affected by shattering and covers a much narrower range of IWC-temperature space than used by [9]. The ensemble model of cirrus ice crystals when convolved with the parameterized PSD [9] has been demonstrated to be physically consistent across the spectrum, from the UV to the radar frequency of 35 GHz [11]. That is, the same microphysical model is applied throughout the spectrum without changing microphysical assumptions to suit particular regions of the spectrum in order to simulate measured radiances. This is an important consideration as global models now have the capability to simulate measured radiances across the spectrum [12, 13], as well as radar reflectivity and lidar backscatter profiles [14].

The parameterization of the bulk optical properties used here has been previously described by [15], and the light scattering methods that have been applied to the ensemble model described above to compute the single-scattering properties between the wavelengths of about 0.2 μm to about 120 μm has been fully described in Ref. [11]. Figure 1 shows the bulk scattering properties ω_0 and g plotted as a function of q_{cf} and wavelength, λ. The bulk optical properties shown in Figure 1 were calculated using 20662 parameterized PSDs obtained from IWC and in-cloud temperature observations derived from a number of field campaigns [11], and the parameterized PSDs were retrieved using the mass-dimensional relationship derived from Ref. [16], which is mass(D)=$0.0257D^2$ (in SI units). This same mass(D) relationship is used in the climate experiments discussed in a later section.

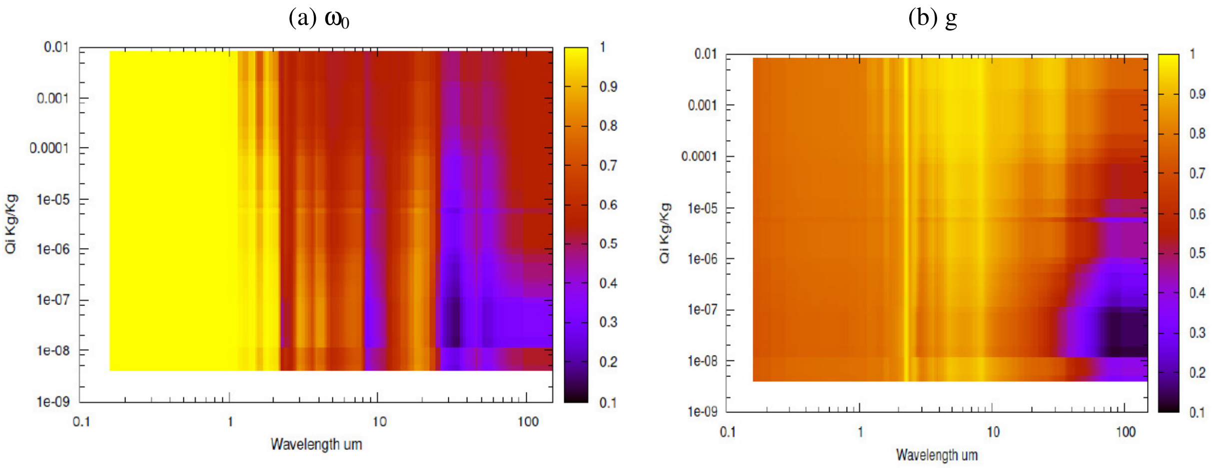

FIGURE 1. The bulk scalar optical properties plotted as a function of q_{cf} and λ showing (a) ω_0 and (b) g.

Figure 1 shows that the bulk scalar optical properties vary strongly as a function of q_{cf} and λ. At the lowest q_{cf} values, the PSDs are narrow, resulting in ω_0 and g being large and small, respectively, at the longer wavelengths. Whilst at the higher q_{cf} values, the PSDs become broader, resulting in lower ω_0 and higher g-values, respectively, again at the more absorbing wavelengths. In Ref. [15] it is shown that the bulk scalar optical properties can be parameterized sufficiently accurately using the following equations.

$$K_{ext}(\lambda,q_{cf})=a_\lambda(q_{cf}) \;;\; K_{sca}(\lambda,q_{cf})=b_\lambda(q_{cf}); \quad g_t(\lambda,q_{cf})=c_\lambda(q_{cf})^{d(\lambda)} \;;\; \omega_0\,(\lambda, qcf)= K_{sca}(\lambda,q_{cf})/\,K_{ext}(\lambda,q_{cf}) \quad (1)$$

In Eq. (1), the constants a, b, c, and d are band-dependent coefficients, and q_{cf} is in units of Kg/Kg. Determining general weights to apply to the ensemble model, so that Eq. (1) can be optimized, is achieved through remote sensing, which is briefly discussed in the next section. The parameterization shown by Eq. (1) is equivalent to that of Ref. [17] in which the bulk optical properties were parameterized as a function of r_e (where r_e is $D_e/2$) and r_e was parameterized as a function of IWC, therefore, the bulk optical properties are also a function of IWC.

Determination of Ensemble Model Weights Using Remote Sensing

The remote sensing section of this short communication has been previously reported in Ref. [18], but a brief summary is given here along with the most pertinent results. To determine which weights to apply to the ensemble model, global radiometric observations in brightness temperature (K) are used at the wavelengths of about 8, 11 and 12 µm obtained from the IIR instrument onboard CALIPSO. The question posed is which weights best minimize the bias between the measurements and forward model when all brightness differences (BTD) between the three wavelengths are aggregated. Although these weights may not actually be what are present in cirrus, they will represent the radiative equivalent ensemble model that best describes the radiometric observations given the model. The forward model used for the simulations is RTTOV (see Ref. [18] for further details), which takes as input ECMWF model fields (temperature and water vapor etc) and the vertical profile of IWC. The vertical profile of IWC is obtained from the DARDAR [19] and 2C-ICE products [20] which are combined to find the averaged vertical profile of IWC. From the ensemble model optical properties the simulated brightness temperatures at the three wavelengths can be obtained from the vertical profiles of the IWC and cloud temperature using the optical properties from Ref. [10]. The parameterization of these optical properties as a function of IWC and cloud temperature is described in Ref. [18].

For this study, the cirrus cases are selected so that the visible optical thickness is between 0.03 and 4. The altitudes are between about 50 – 450 hPa. The cloud fraction is unity; aerosol contaminated profiles are removed using the DARADAR cloud mask, and only cases over the ocean are considered to reduce uncertainties in surface emission. With these criteria for case selection, a total of 26791 profiles are selected from one week in February and August 2010, and the cases are distributed from the North Pole to the Antarctic, with the majority of cases located in the tropics. A full description of case selection and methodology can be found in Ref. [18].

The process of minimizing the biases as a function of weighting the ensemble model at each bin size was achieved through an iterative process, and the resulting bias minimization can be seen in figure 2. Also shown in figure 2 are the other RTTOV parameterizations, and these depend on the profile of D_e as well as IWC. The profile of D_e is also a DARADAR and 2C-Ice product. The other RTTOV parameterizations are defined in Ref. [18].

Figure 2 shows that on the left hand-side of the figure five out of the six standard RTTOV parameterizations are biased in latitude. However, the RTTOV parameterization that is not as biased is DEH, which is a vertical profile of hexagonal ice columns as a function of D_e. Although, in Ref. [21] it was shown that the hexagonal ice column was not physically consistent when compared against simultaneous measured cirrus radiances in the short-wave and long-wave. Therefore, it would be expected that this parameterization would fail if the same method was applied to both short-wave and long-wave measurements simultaneously. The parameterizations on the right-hand side of Figure 2 are parameterizations based on the ensemble model labelled Bx.xxxx, where x.xxxx represent different pre-factors in the mass-dimensional relationship when applied to the PSD parameterization of Ref. [7]. However, the exponent is kept constant at a value of 2 in accord with the literature [16] and is consistent with the global model cirrus microphysics scheme. The larger the pre-factors, the denser the ice particles; therefore, to conserve ice mass fewer larger ice particles are required. However, Figure 2 shows that these tend to be too transmitting. However, the lower the pre-factor the less dense the particles are and so therefore more larger particles are required to conserve ice mass, and, thus, these tend to be less transmitting, as shown by Figure 2.

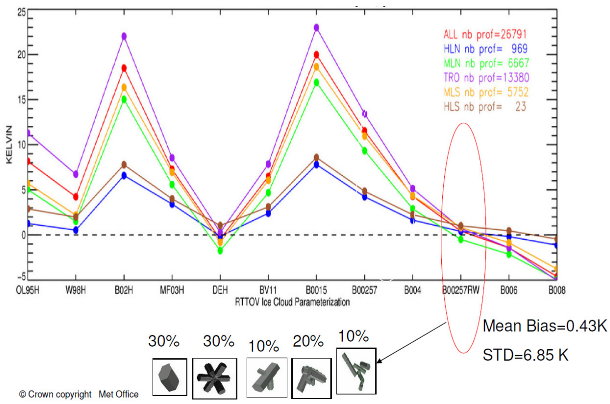

FIGURE 2. The zonally averaged mean brightness temperature biases between IIR measurements and forward model as a function of RTTOV parameterization. The zonally averaged mean biases are color-coded and are defined by the key in the top-right of the figure. Red is for all zones; blue, high latitude north; green, Mid-latitude north; purple, tropics; light brown, mid-latitude south; and dark brown, high-latitude south, after Ref. [18].

The prefactor of B0.0257 is weighted towards the hexagonal ice columns and bullet-rosettes contained in the ensemble model, and this results in the cloud being too cold relative to the observations. However, changing the weighting of the ensemble model at each size bin whilst conserving the pre-factor in accord with Ref. [16] results in the parameterization labeled B0.0257RW (encompassed by the red ellipse shown in Figure 2) and this was achieved using the following weights applied to the ensemble model at each size bin: 30% hexagonal columns, 30% six-branched bullet-rosettes, 10% three-branched hexagonal ice aggregates, 20% five-branched hexagonal ice aggregate, and, finally, 10% eight-branched hexagonal ice aggregates. This habit mixture model is the best fit to the radiometric measurements in the terrestrial window region. It remains to be seen if this fit is as good when more wavelengths are added, including wavelengths in the solar region. The mean bias in the best-fit parameterization is just 0.43 K but with a standard deviation of 6.85 K, and it should be noted that this removes the dependence of the mean bias on latitude unlike five of the standard RTTOV parameterizations. Some of these standard RTTOV parameterizations might well be used in climate models; if so, those models will have a latitudinal bias in their predicted cirrus radiative long-wave fluxes. A recent study by Ref. [22] demonstrates the importance of 3D radiative effects at the IIR wavelengths used here, and, therefore, some of the STD (i.e., Standard Deviation) observed might be due to the 3D effects not accounted for in the plane-parallel RTTOV model. It is, therefore, important to find a fast parameterization of the 3D radiative effect that could be applied to a plane-parallel model such as RTTOV.

Figure 2 demonstrates that, through the ensemble model, a radiatively-equivalent cloud to the observations can be found, and, as such, this radiative parameterization can be applied to a climate model as it has been demonstrated to be globally representative. Moreover, it is consistent with the assumed microphysics in the global climate model. The next section describes the impact of the best-fit parameterization on the Met Office Unified Global Atmosphere 6.0 configuration.

Impact of the Parameterization in the Met Office Unified Global Atmosphere Model Configuration 6

The optimal weighting of the ensemble model derived in the previous section is now applied to the Met office Unified Global Atmosphere model configuration 6.0. In the 20 year averaged experimental climate runs, the cloud microphysics scheme assumes the mass-dimensional relationship derived by Ref. [16], that is $m(D)=0.0257D^2$, and all other moments that contribute to the cirrus microphysics and cloud evolution such as fall speed and capacitance are derived from the moment estimation parameterization derived by Ref. [7]. In the experimental climate runs, the radiation scheme is completely consistent with the assumed microphysics with respect to the mass-dimensional relationship and PSDs. The experimental climate run is compared against the control 20 year averaged climate run, and the control is the same configuration as the experiment but assumes the same cirrus microphysics and cirrus radiation scheme as the current Met Office operational global model. In the control, the cirrus microphysics scheme assumes the PSD parameterization developed by Ref. [9], and the mass-dimensional relationship developed by Brown and Francis [23]. The ice radiation scheme assumed in the control model is from Ref. [1]. The control climate run is inconsistent with respect to PSDs, mass-dimensional relationships and, therefore, all other moments that are important contributions to cloud ice evolution within the model. On the other hand, the experimental run is consistent. The cirrus radiation parameterization assumed in the experimental run corresponds to the label B0.0257RW shown in Figure 2.

To compare results from the control and experiment, the 20 year averaged TOA outgoing short-wave and long-wave fluxes are compared against the EBAF CERES product [24], and the model predictions of the temperature structure of the atmosphere are compared against the ERA-Interim ECMWF analysis [25]. The comparisons are shown for the summer season (June-July-August). Figure 3 shows results for the short-wave flux, and Figure 4 shows results for the outgoing long-wave flux. The flux is in units of Wm^{-2}.

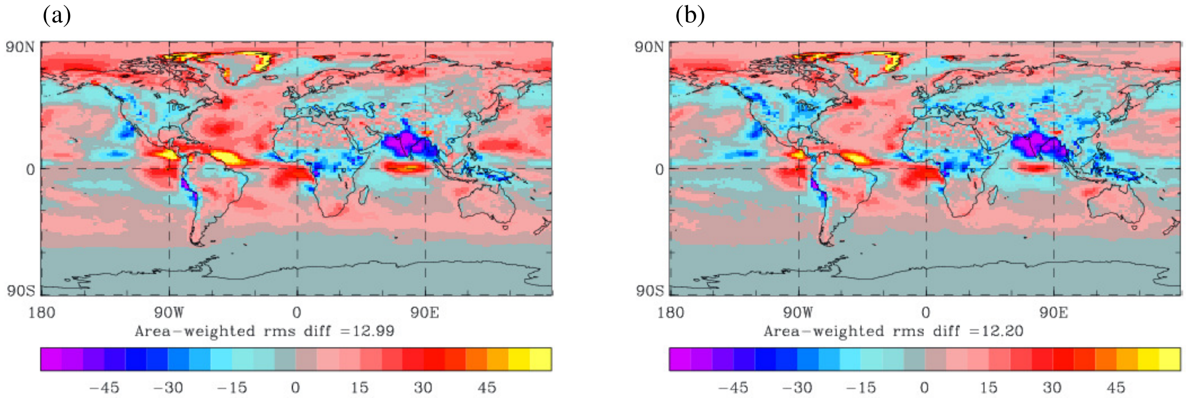

FIGURE 3. The twenty year averaged reflected short-wave flux at TOA for June-July-August (a) control model (b) experiment.

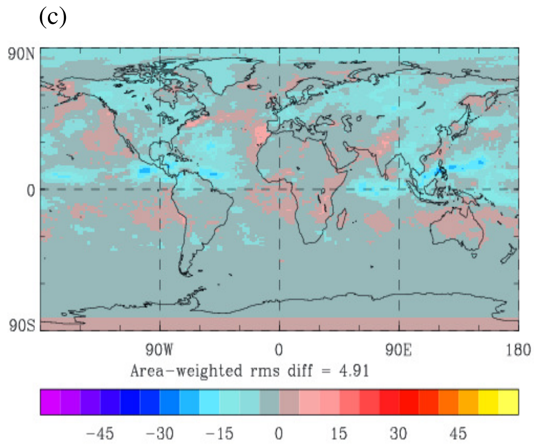

FIGURE 3C. The difference in the reflected short-wave flux at TOA between the experiment and control.

Figure 3 (a-c) shows that the cloud in the consistent run (i.e., Figure 3b) is generally less bright than in the control. This leads to distinct improvements in the tropics with the brightness substantially reduced and in more agreement with the EBAF product, this is also the case in the sub-tropics, both North and South. The area-weighted root mean square difference (rms) is also reduced in the experiment relative to the control by 0.79 Wm^{-2}. The reason for this difference could be due to the radiation scheme. In that the control run, the assumed D_e is too small, and, so, the mass extinction is too large. Hence, this will increase the reflected short-wave flux. As a consequence, the outgoing long-wave flux in the control should be reduced relative to the EBAF product. This effect is shown in Figure 4.

As a consequence of the ice clouds being less bright in the tropics, the outgoing long-wave is increased in the experiment relative to the control as shown by Figure 4c and Figure 4b. However, in general, the experiment increases transmission in the long-wave relative to the control, but this does reduce the area-averaged rms value relative to the EBAF product when compared against the control by 0.59 Wm^{-2}. However, the change in the OLR in the experiment is not as dramatic as the short-wave change shown in Figure 3 (a-c). This is because, in the long-wave, the emission is determined also by cloud-top altitude and surface emission, as well as atmospheric emission below and above the cloud. The consequence for the temperature structure of the atmosphere due to this change in the short-wave and long-wave is shown in Figure 5.

(a) (b)

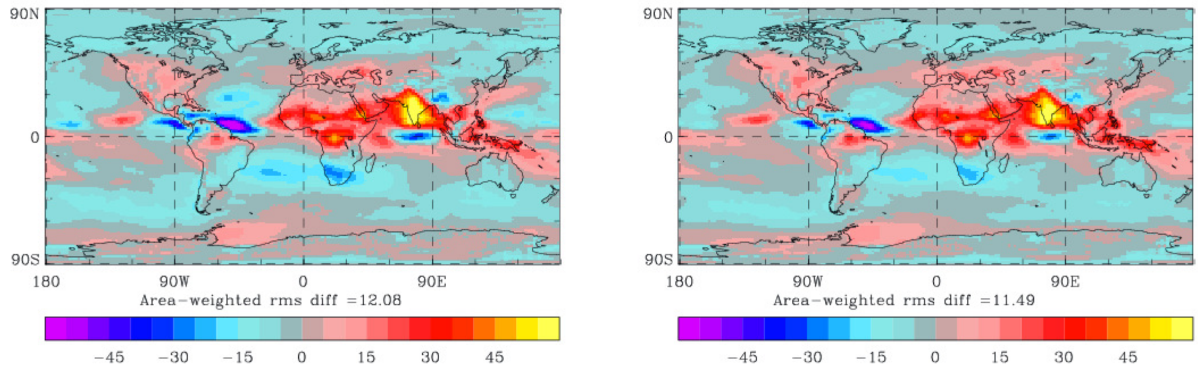

FIGURE 4. The twenty year averaged outgoing long-wave flux at TOA for June-July-August (a) control model (b) experiment

(c)

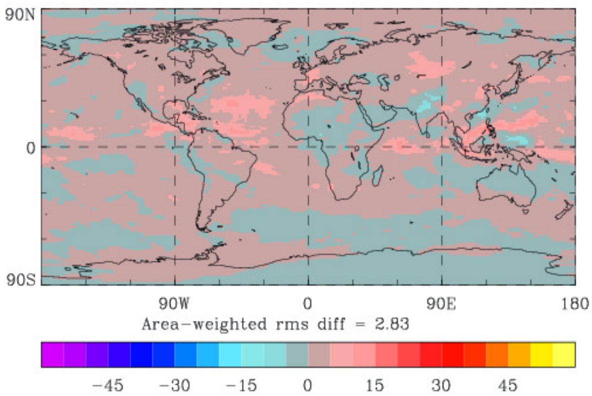

FIGURE 4C. The difference in the outgoing long-wave flux at TOA between the experiment and control.

(a) (b)

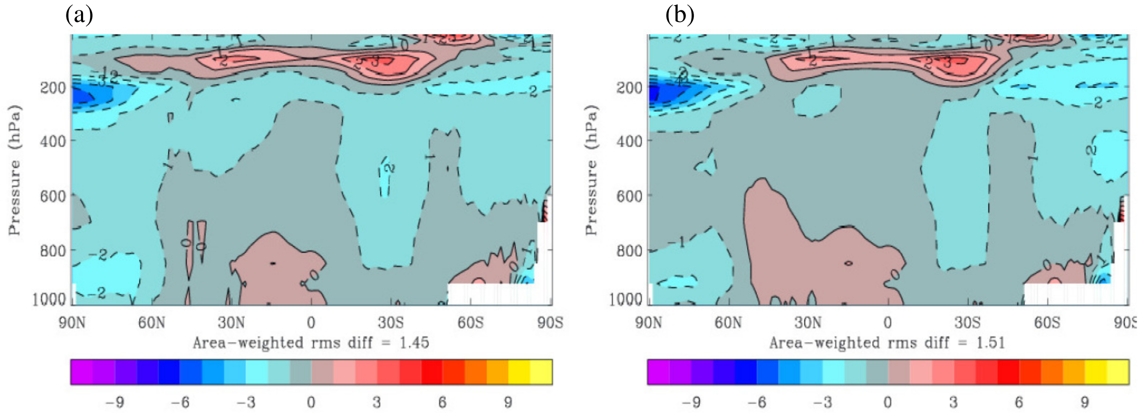

FIGURE 5. The twenty year zonally averaged temperature differences between (a) control – ERA Interim analysis and (b) experiment – ERA Interim analysis for June-July-August. The temperature differences are in units of K.

Figure 5 shows an improvement in the temperature structure of the tropical troposphere in the case of Figure 5(b) which is the consistent model. The inconsistent model shows the classic over cooling of the tropical troposphere which has been a long-standing problem in the global model. Moreover, the consistent approach also reduces the extent of the warming at the tropical tropopause as shown by Figure 5 (b). However, the area-averaged rms in the case of the consistent approach has increased by 0.06 K. This is due to the excessive cooling in the Arctic at a height of about 200 hPa and over the Antarctic at the same height. The consequences of a more unified approach between cirrus microphysics and radiation are summarized in the next section.

SUMMARY

A unified approach between cirrus microphysics in a global atmospheric model, space-based remote sensing, and the cirrus ice optics in the radiation scheme has led to an improvement in the short-wave and long-wave fluxes at TOA as measured by the area-averaged rms values relative to the EBAF product. This improvement is especially noteworthy in the tropics with respect to the short-wave reflection at TOA. As a consequence, this changed the temperature structure of the atmosphere to neutral values in the tropical troposphere and reduced the extent of the tropical tropopause warming relative to the ERA-Interim ECMWF analysis. This short-communication has also shown that, at least in the terrestrial window region, the bias in the brightness temperature differences can be eliminated by finding a suitable weighted habit mixture model of cirrus ice crystals. Although such a weighting may not be what is actually present in cirrus, the important thing is to attain the radiative equivalent which is the essential criteria for a radiation scheme in a climate model. Traditionally, the treatment of cirrus microphysics and radiation in climate models has been separate, but in reality the processes are coupled. As a consequence, this has led to inconsistency between the cloud and radiation schemes in climate models. Here consistency has been maintained through the use of the same mass-dimensional relationship and PSDs throughout the remote sensing and radiation and cirrus microphysics schemes. Due to the moment estimation parameterization being referenced to the GCM model prognostic variable q_{cf}, all other moments are also consistent between the radiation and cirrus microphysics cloud schemes. A further consequence of this is that future climate model simulation of satellite observations from across the spectrum can be achieved consistently.

REFERENCES

1. J. M. Edwards, S. Havemann , J.-C. Thelen, and A. J. Baran, *J. Atmos. Res.,* **83**, 19-35 (2007).
2. P. Yang, and K. N. Liou, *Contr. Atmos. Phys.*, **71**, 223-248 (1998).
3. P. R.Field, R. Wood, P. R. A. Brown, P. H. Kaye, E. Hirst, R. Greenaway, and J. A. Smith, J. Atmos. Oceanic Technol., 20, 249– 261(2003).
4. A. V. Korolev, E. F. Emery, J. W. Strapp, S. G. Cober, and G. A. Isaac, *J. Atmos. Ocean. Tech*., **30**, 2527-2553 (2013).
5. Intergovernmental Panel on Climate Change, *Climate Change 2013 - The Physical Science Basis: Contribution of Working Group I to the Fourth Assessment Report of the IPCC*, Cambridge University Press (2013).
6. A. J. Baran, and L.-C. Labonnote, *Q. J. R. Meteor. Soc.,* **133**, 1899-18912 (2007).
7. Yang, P., L. Bi, B. A. Baum, K.-N. Liou, G. Kattawar, M. Mishchenko, and B. Cole, *J. Atmos. Sci*., **70**, 330-347 (2013).
8. Baum, B. A., P. Yang, A. J. Heymsfield, A. Bansemer, A. Merrelli, C. Schmitt, and C. Wang:, *J. Quant. Spectrosc. Radiat. Transfer,* **146**, 123-139, doi:10.1016/j.jqsrt.2014.02.029 (2014).
9. P. R. Field, A. J. Heymsfield, and A. Bansemer, *J. Atmos. Sci*., **64**, 4346-4365 (2007).
10. R. A. Houze, P. V. Hobbs, P. H. Herzegh, and D. B. Parsons, J. Atmos. Sci., **36**, 156–162 (1979).
11. Anthony. J. Baran, Richard Cotton, Kalli Furtado, Stephan Havemann, Laurent-C Labonnote, Franco Marenco, Andrew Smith, Jean Claude-Thelen, Q.J.R. Meteorol. Soc., **140**, 1039-1057 (2014).
12. M. A. Ringer, J. M. Edwards and A. Slingo, Q.J.R. Meteorol. Soc., **129**, 1169-1190 (2003).
13. Jean Claude-Thelen, J. M. Edwards, Q.J.R. Meteorol. Soc., **139**, 1665-1679 (2013).
14. A. Bodas-Salcedo, and co-authors, *Bull. Amer. Meteor. Soc.*, **92**, 1023–1043 (2011).
15. Baran, A., P. Hill, K. Furtado, P. Field, and J. Manners, 2014: A Coupled Cloud Physics-Radiation Parameterization of the Bulk Optical Properties of Cirrus and its Impact on the Met Office Unified Model Global Atmosphere 5.0 Configuration. J. Climate. doi:10.1175/JCLI-D-13-00700.1, in press.
16. R. J. Cotton, P. R. Field., Z. Ulanowski., P. H. Kaye, E Hirst, R. S. Greenaway, I. Crawford, J. Crosier, and J. Dorsey, Q. J. Roy. Meteor. Soc., **139**, 1923–1934 (2013).

17. G. M. McFarquhar., S. Iacobellis, and R. C. J. Somerville, *J. Clim*., **16**, 1643-1664 (2003).
18.. J. Vidot, A. J. Baran, and P. Brunel, J. *Geophys. Rev*., in review.
19. J. Delanoë, and R. J. Hogan, *J. Geophys. Res*., **115**, D00H29 (2010).
20. M. Deng., G. G. Mace, Z. Wang,, and H. Okamoto, *J. Geophys. Res*., **115**, D00J15 (2010).
21. A. J. Baran, and P. N. Francis, *Q. J. R. Meteorol. Soc*., **130**, 763–778 (2004).
22. T. Fauchez, C. Cornet, F Szczap, P. Dubuisson1 and T. Rosambert, *Atmos. Chem. Phys*., **14**, 5599–5615 (2014).
23. A. R. P. Brown, and P. N. Francis, *J. Atmos. Ocean. Tech*., **12**, 410-414 (1995).
24. N. G. Loeb, B. A. Wielicki, D. R. Doelling, G. L. Smith, D. F. Keyes, S. Kato, N. Manalo-Smith, and T. Wong, J. Climate, 22, 748766, doi10.1175/2008JCLI2637.1 (2009).
25. D. P. Dee, and co-authors, Q. J. Roy. Meteor. Soc., **139**, 1923–1934 (2011).